Enhancement of Brownian motion for a chain of particles in a periodic potential

Tommy Dessup, Christophe Coste, and Michel Saint Jean
Laboratoire "Matière et Systèmes Complexes" (MSC), UMR 7057 CNRS, Université Paris–Diderot (Paris 7), 75205 Paris Cedex 13, France

(Received 29 November 2017; published 2 February 2018)

The transport of particles in very confined channels in which single file diffusion occurs has been largely studied in systems where the transverse confining potential is smooth. However, in actual physical systems, this potential may exhibit both static corrugations and time fluctuations. Some recent results suggest the important role played by this nonsmoothness of the confining potential. In particular, quite surprisingly, an enhancement of the Brownian motion of the particles has been evidenced in these kinds of systems. We show that this enhancement results from the commensurate effects induced by the underlying potential on the vibrational spectra of the chain of particles, and from the effective temperature associated with its time fluctuations. We will restrict our derivation to the case of low temperatures for which the mean squared displacement of the particles remains smaller than the potential period.

DOI: 10.1103/PhysRevE.97.022103

I. INTRODUCTION

Transport in very confined channels in which the particles are distributed along an ordered file and cannot cross each other has been extensively studied. The *mean squared displacement* (MSD) of these particles in an infinite system scales as the square root of time. This characteristic scaling for correlated particles is known as *single file diffusion* (SFD). In finite systems with periodic boundary conditions, this SFD is a transient regime which is followed by the Fickian diffusion of an effective particle with the mass of the whole system. In relevant studies, the particles interact as hard spheres [1–3] or with finite range interactions [4–6], and the considered systems are either strictly one dimensional or a set of particles confined in a narrow smooth channel.

However, in actual systems in which SFD occurs, the transverse confining potential may involve static corrugations and time fluctuations. It is the case at the molecular scale for intracellular motions through biological membranes [7,8], ultrafiltration through carbon nanotubes [9], or through zeolites [10]. This situation can also be seen at a larger scale. It occurs in the motion of colloidal particles in microfluidic devices [11–14] or in systems of coupled particles in which a chain of particles diffuses in the potential created by the other ones as in superfluid ^{4}He [15], or Bose-Einstein condensates [16] confined in circular cells and in type II superconductor stripes [17–20].

This has motivated a number of specific simulations and experimental studies in such configurations and unexpected dynamics has been observed. For instance, the relative motions of coupled particles submitted to an underlying potential can display parametric resonances [21–23]. A surprising effect has been exhibited in macroscopic Wigner islands. In these patterns, in which the particles are distributed in concentric shells, it has been shown that the particles of the outer shell diffuse more quickly than the same number of particles in a smooth annulus of the same radius and same width [24]. The authors attribute this "diffusion enhancement" to the effect of the fluctuating underlying potential applied by the particles of the inner shells on those of the outer one. Note that this enhancement of the Brownian motion contrasts to the case of a single particle for which an underlying periodic potential induces a slowing down of the diffusion [25–28]. Since these Wigner islands can be considered as a model system of a chain diffusing on a fluctuating underlying potential, these effects could be observed in various other contexts in which a chain diffuses in a channel with corrugations.

To understand the origins of this enhancement of the MSD in this intermediate regime and the role played by the confinement potential, corrugation is therefore an important issue. While the diffusion of a single particle in a corrugated channel has been largely discussed [29–33], the results concerning the diffusion of a chain of interacting particles submitted to an underlying potential are more rare. Some papers have considered the longitudinal diffusion of a chain over a distance that is large with respect to the potential period in the case of hard sphere interactions between particles [34] or of finite range interactions [29,35]. The case of diffusion over distances smaller than the period of the underlying potential has also be discussed [36,37], and commensurability between the chain and the underlying potential has been considered in Refs. [38,39]. All these theoretical studies consider a static underlying potential. However, it seems of interest to study also a fluctuating underlying potential in order to fully describe the effects of thermal fluctuations of the underlying potential that occur in actual systems.

In this article, we propose a mechanism for the enhancement of Brownian motion resulting from the commensurate effects induced by the underlying potential on the vibrational spectra of a chain and from the effective temperature associated with its fluctuations. We will restrict our derivation to the case of low temperatures for which the MSD remains smaller than the potential period.

In Sec. II we recall the main steps of the derivation of the transport coefficients from the phonon spectrum of a free single file of particles, without any underlying potential. In Sec. III we show how a band gap opening induced by a static underlying

potential in the phonon spectrum can explain the enhancement of the particles' dynamics. The effect of the fluctuations of this potential on the transport coefficients is discussed in Sec. IV. Lastly, the results of these theoretical predictions are compared to those obtained by simulations or in previous experiments on Wigner islands in Sec. V. In Appendix A we recall how the phonon spectrum allows the calculation of the particles' MSD. In Appendix B, a complementary study justifies the description of the Brownian motion of two interacting chains as that of a single chain in the periodic and fluctuating potential created by the other one.

II. SINGLE FILE DIFFUSION AND VIBRATIONAL MODES

The diffusion of interacting particles organized in a quasi-one-dimensional chain is characterized by a subdiffusive correlated regime. In this regime the MSD of a particle scales as the square root of time, instead of the linear time scaling of ordinary diffusion. The first theoretical approaches have explained this behavior for hard spheres [1–3] whereas the case of finite range interactions has been considered only recently [4–6].

In our previous study [6], we have shown that the SFD in a system with finite range interactions may be fully described in a very simple manner by considering the particles' motions as a superposition of the diffusive motions of their vibrational normal modes. Our calculations give an analytical description of SFD in finite systems that is in excellent agreement with experiments and simulations [6,40]. Moreover, in the thermodynamic limit (particle number $N \to \infty$ at finite density) we recover the result of Refs. [4,5], but with much simpler calculations.

Let us recall the main steps of this fruitful approach. The SFD of a chain of N identical particles of mass m may be described with a set of N coupled Langevin equations, where the thermal bath of temperature T is accounted for by a dissipation constant γ and an uncorrelated Gaussian noise on each particle (see Sec. V). This set of coupled equations is solved with a projection onto the phonon basis, with wave vectors q, frequencies $\omega(q)$, and amplitude $X(q,t)$. The dynamics of each phonon is given by the Langevin equation for a damped harmonic oscillator with dissipation γ and a characteristic frequency equal to $\omega(q)$. Because of the orthogonality of the phonon basis, the thermal noises on each phonon is uncorrelated between them (see Ref. [6] and Appendix A). Therefore, the amplitude fluctuation of each phonon $\langle \Delta X^2(q,t)\rangle$ scales as t^2 in the initial ballistic regime and eventually reaches a saturation value $k_BT/[m\omega^2(q)]$ at a long time (with k_B the Boltzmann constant).

The crossover time between the ballistic and the saturated regime decreases with $\omega(q)$ for a phonon of wave number q. The zero wave-number mode which is linked to rotational invariance (in finite systems with periodic boundary conditions) or translational invariance (in the thermodynamic limit) has a peculiar behavior because $\omega(q=0)=0$. This Goldstone mode diffuses as a free effective particle, of mass Nm in finite systems, so that $\langle \Delta x^2(q=0,t)\rangle$ scales linearly with time at a very long time.

In this description, the particles' MSD $\langle \Delta x^2(t)\rangle$ is obtained by adding all the phonon contributions, taking into account their relative weights. In particular, we have shown that the SFD correlated regime results from the gradual decrease of the number of modes which are still in their ballistic regime as the time t increases, since the evolution of $\langle \Delta x^2(t)\rangle$ is dominated by the contributions of the modes that have not reached their saturation. The details of this derivation can be found in Ref. [6] and we give below only a brief summary of its main results.

For the sake of simplicity, let us first consider an overdamped system. At a given time t, the unsaturated modes are such that $t < \gamma/\omega^2(q)$ and correspond to $q < (\gamma/t)^{1/2}(k/m)$ if we assume the Debye approximation $\omega(q) = q\sqrt{k/m}$, where k is the stiffness of the interparticle interaction. The number $n(t)$ of unsaturated modes is therefore $n(t) \sim 2(N/2\pi)(\sqrt{\gamma}/\sqrt{tk/m})$. On the other hand, the behavior of $\langle \Delta X^2(q,t)\rangle$ in the intermediate time between the ballistic and the saturated regime is found to be $[2k_BT/(Nm\gamma)]t$ [6]. The MSD is thus estimated as

$$\langle \Delta x^2(t)\rangle \sim \frac{2k_BT}{Nm\gamma} t\, n(t) \sim \frac{2k_BT}{Nm\gamma} t \frac{2N}{2\pi}\sqrt{\frac{m\gamma}{kt}} = \frac{2k_BT}{\pi\sqrt{mk\gamma}} t^{1/2}. \tag{1}$$

Let us now consider an underdamped system. In this latter case, $n(t) \sim 2(N/2\pi)(1/t\sqrt{k/m})$ and the behavior of $\langle \Delta X^2(q,t)\rangle$ before the saturated regime is found to be $(k_BT/Nm)t^2$. The MSD is thus estimated as

$$\langle \Delta x^2(t)\rangle \sim \frac{k_BT}{Nm} t^2\, n(t) \sim \frac{k_BT}{\pi\sqrt{mk}} t. \tag{2}$$

Note that in this framework, the long time behavior of the MSD in finite systems results from the behavior of the zero wave-number mode since this mode eventually dominates the dynamics, which implies that $\langle \Delta x^2(t)\rangle$ eventually scales as t.

Therefore, the transport coefficients and the crossover times are determined as functions of the system parameters (particle number, stiffness of the interparticle interaction, temperature, etc.). For an overdamped dynamics, Eq. (1) predicts a subdiffusive SFD behavior for finite systems, with a mobility $F_0 \equiv \langle \Delta x^2(t)\rangle/t^{1/2}$ that reads

$$F_0 = \frac{2k_BT}{\pi}\sqrt{\frac{2}{m\gamma k}}. \tag{3}$$

For an underdamped dynamics, Eq. (2) predicts a diffusive behavior with a diffusivity $D_0 \equiv \langle \Delta x^2(t)\rangle/t$ that reads

$$D_0 = \frac{k_BT}{\pi\sqrt{mk}}. \tag{4}$$

These estimates are found to be in excellent quantitative agreement with the results obtained by simulation and experiments as well [6,41].

Let us emphasize the importance of the modes with frequencies located in the middle of the acoustic branch in these nontrivial collective effects at an intermediate time. We will see that this point is also essential to understanding the effect of an underlying potential on the SFD. In what follows, we generalize this method to calculate the diffusion coefficient and the mobility of particles in a chain diffusing over a periodic potential.

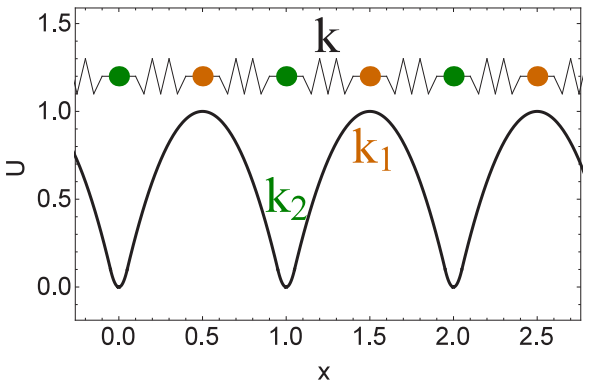

FIG. 1. Schematic representation of the equilibrium position of a chain of identical masses m coupled by springs of stiffness k and interacting with an underlying periodic potential with two particles for each period. The absolute value of the local curvature is k_1 (k_2) at the maxima (minima). In this figure, the potential period is taken as the unit length.

III. VIBRATIONAL MODES WITH A STATIC UNDERLYING POTENTIAL

Let us first consider the simplest case in which the interparticle distance d is equal to the period of the underlying potential, the barrier amplitude being E_0. In this case, at low temperature ($k_BT \ll E_0$), the equilibrium configuration corresponds to one particle trapped in each potential minimum. The translation invariance is therefore broken, the Goldstone mode disappears, and $\omega^2(q=0)$ takes a finite value. The resulting local curvature k' at the potential minimum induces a constant shift k'/m of the values $\omega^2(q)$ calculated without the underlying potential. The finite value of $\omega^2(q=0)$ results in the saturation of $\langle \Delta X^2(q=0)\rangle$ at a long time and therefore eventually in a finite value of $\langle \Delta x^2(t)\rangle$. However, this regime may be hidden in a practical case since for a small stiffness k' the crossover time can be very large. Therefore, the longitudinal MSD will be very similar to that of the free chain, with a somewhat smaller diffusion coefficient D and mobility F.

A more interesting situation happens when the period of the underlying potential is twice the interparticle distance. For instance, it corresponds to the "magic numbers" configurations of the Wigner islands for which "diffusion enhancement" has been observed [24,42] and which will be discussed in Sec. V. We consider a system of $2N$ interacting particles regularly located at the maxima and minima of an underlying potential $U(x)$, assuming periodic boundary conditions at the ends of this cell of length $2Nd$. This equilibrium position is sketched in Fig. 1, and the condition for its stability will be eventually established from the vibrational modes of the system. We assume a harmonic interparticle interaction, characterized by a uniform stiffness k and limited to first neighbors only. The absolute values of the local curvatures of the underlying potential at its maxima and minima are denoted k_1 and k_2 (see Fig. 1).

Such a system can be considered as a set of N cells with two particles in each cell. The small displacements near the equilibrium positions of the particles of the jth cell are denoted $x_j^\alpha(t)$, where the greek index $\alpha \in \{1,2\}$. Choosing the x axis origin in such a way that $U(0)$ is a local minimum, the positions of the particles are thus $(2j+1)d + x_j^1(t)$ and $2jd + x_j^2(t)$ and with $j = 1,\ldots,N$. The dynamical equations for the jth cell particles are thus

$$\begin{cases} m\ddot{x}_j^1 = k\left(x_j^2 + x_{j-1}^2 - 2x_j^1\right) + k_1 x_j^1, \\ m\ddot{x}_j^2 = k\left(x_{j+1}^1 + x_j^1 - 2x_j^2\right) - k_2 x_j^2. \end{cases} \tag{5}$$

Since the system is periodic, the solutions can be written in a Fourier series,

$$X_\alpha(s,t) = \sum_{j=1}^{N} x_j^\alpha(t) e^{-i\frac{2\pi}{N}sj}, \quad x_j^\alpha(t) = \frac{1}{N}\sum_{s=1}^{N} X_\alpha(s,t) e^{i\frac{2\pi}{N}sj}. \tag{6}$$

Therefore, the dynamic equations become

$$\begin{cases} \ddot{X}_1 = \dfrac{k}{m}(X_2 + X_2 e^{-i\frac{2\pi}{N}s} - 2X_1) + \dfrac{k_1}{m}X_1, \\ \ddot{X}_2 = \dfrac{k}{m}(X_1 e^{i\frac{2\pi}{N}s} + X_1 - 2V) - \dfrac{k_2}{m}X_2. \end{cases} \tag{7}$$

The normal modes are found by diagonalizing the dynamic matrix $\mathbb{M}$,

$$\mathbb{M} \equiv \frac{1}{m}\begin{pmatrix} k_1 - 2k & k(1+e^{-i\frac{2\pi}{N}s}) \\ k(1+e^{i\frac{2\pi}{N}s}) & -k_2 - 2k \end{pmatrix}. \tag{8}$$

The eigenfrequencies are

$$\omega_\pm^2[q(s)] = \frac{1}{2m}[4k + (k_2 - k_1) \pm \sqrt{(k_1+k_2)^2 + 16k^2\cos^2[q(s)]}], \tag{9}$$

with $q(s) = 2\pi s/(2N)$ for $s = 1,\ldots,N$, and the eigenvectors are

$$\mathbf{V}_\pm = \frac{1}{\mathcal{N}_\pm}\begin{pmatrix} \frac{(k_1+k_2)\pm\sqrt{8k^2+(k_1+k_2)^2+8k^2\cos(q)}}{2(1+e^{iq})k} \\ 1 \end{pmatrix}, \tag{10}$$

where $\mathcal{N}_\pm$ is a normalization factor.

The smallest eigenfrequency is obviously $\omega_-(q=0)$, and the equilibrium configuration is stable if this frequency is real, which requires

$$\omega_-^2(q=0) = \frac{1}{2m}[4k + (k_2 - k_1) - \sqrt{(k_1+k_2)^2 + 16k^2}] > 0. \tag{11}$$

Therefore, for a given potential characterized by k_1 and k_2, the considered configuration is at equilibrium if and only if the interparticle stiffness k is higher than a critical stiffness k_c, where

$$k_c \equiv \frac{k_1 k_2}{2(k_2 - k_1)}. \tag{12}$$

Since k_c has to be a finite positive stiffness, the stability of a configuration such as in Fig. 1 requires a periodic potential with asymmetric extremal curvatures, such that the absolute value of the curvature at a maximum (k_1) is less than the curvature at a minimum (k_2). This configuration is otherwise always unstable, except for the rigid chain (k_c infinite). In what follows, this kind of periodic potential will be referred to for brevity an *asymmetric potential*.

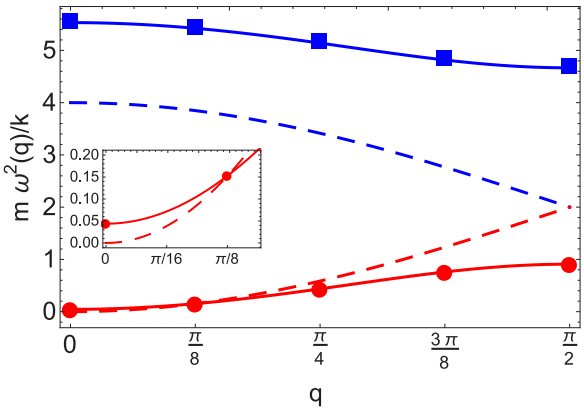

FIG. 2. Dimensionless squared eigenfrequencies $m\omega^2(q)/k$ for acoustical (red) and optical (blue) modes as a function of the dimensionless wave number q. The dashed lines correspond to the free chain and the solid lines to the chain in an underlying potential. The blue squares and red disks indicate the eigenfrequencies of a finite system with $2N = 16$ particles. The stiffnesses are $k_1 = 1.09\ k$ and $k_2 = 8k/3$ (hence $k = 1.08k_c$). The inset shows a zoom at small wave number for the acoustical modes.

In Fig. 2 we plot the dispersion relations $\omega^2(q)$ given by Eq. (9). In order to emphasize the effect of the underlying potential, the corresponding plot for a free chain is displayed in dashed lines. Two strong effects are evidenced. Since the unit cell includes two particles, the corresponding first Brillouin zone is divided by two. Therefore, the underlying potential induces the folding of the free chain dispersion curve and opens a forbidden band at the zone borders of the reduced Brillouin zone, with a width that is proportional to $(k_1 + k_2)$ [see Eq. (9)]. Moreover, as in the previous case, the breaking of translational invariance induced by the underlying potential implies a finite (nonzero) value of $\omega_-(q = 0)$. In the limiting case $k \approx k_c$, it reads

$$m\omega_-^2(q) \overset{q\to 0}{\sim} m\omega_-^2(q=0) + \frac{2k^2}{\sqrt{(k_1+k_2)^2+16k^2}}q^2, \quad (13)$$

with $\omega_-(q = 0) \approx 0$.

IV. BROWNIAN MOTION OF A CHAIN IN AN UNDERLYING POTENTIAL

A. Effect of the band gap on the particles' MSD

Let us now consider a chain of particles that interacts with the periodic underlying potential with asymmetric extremal curvatures of Sec. III (see Fig. 1) and with a thermal bath characterized by a temperature T and a dissipation coefficient γ.

The analysis of the MSD $\langle \Delta x_\alpha^2(t)\rangle$ as the superposition of the phonons' MSD $\langle \Delta X_\alpha^2(q,t)\rangle$ (see Sec. II and Ref. [43]) and the previous calculation of the phonon spectrum of a chain in an underlying potential (Sec. III) suggests some qualitative effects of the underlying potential on the particle diffusion. Since $\omega(q = 0)$ has a small finite value, the MSD does not scales as t at a long time as for a free chain, but reaches a very large saturation value $k_BT/[m\omega^2(q = 0)]$ at a very large crossover time of order $1/\omega(q = 0)$ or $\gamma/\omega(q = 0)^2$, depending on the dissipation regime.

The most important effect of the band gap concerns the SFD correlated regime. Indeed, this intermediate regime is mainly led by the dynamics of the phonons in the middle of the Brillouin zone. These phonons are precisely those whose frequencies are the most strongly affected by the underlying potential. In particular, the frequencies of the acoustical branch are smaller than that of the free chain. Therefore, we can expect that the corresponding phonons' MSD saturates later than without an underlying potential, which implies a greater contribution $\langle \Delta X_\alpha^2(q,t)\rangle$ of these phonons, hence an increase of the transport coefficients in the SFD regime. This effect on the correlated regime will be maximum for the largest available band gap, which happens when the stiffness k tends to k_c. Therefore, in the following, we restrict our calculations to the case $k = k_c$. In order to obtain quantitative expressions of the transport coefficients, we process in a similar fashion as for the free chain. The details of the calculations of $\langle \Delta X_\alpha^2(q,t)\rangle$ and $\langle \Delta x_\alpha^2(t)\rangle$ are given in Appendix A.

In Fig. 3 we display the MSD as a function of time for a system of 16 particles. The MSD of some eigenmodes $\langle \Delta X_\alpha^2(q,t)\rangle$ is shown in Fig. 3(a). At very small times, all contributions are identical. The MSD of optical modes is the first to saturate at very small and very close values [almost indistinguishable—see the blue lines in Fig. 3(a)]. After the saturation of all optical modes, the MSD of the acoustical

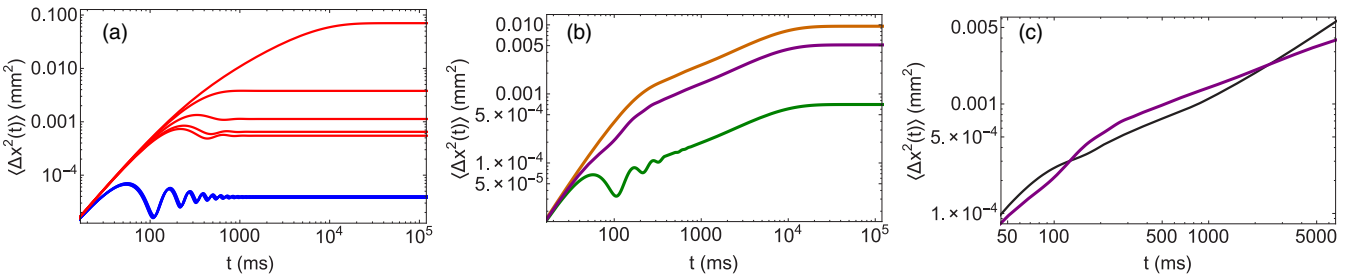

FIG. 3. MSD (mm^2, logarithmic scale) as a function of time (ms, logarithmic scale). (a) Some eigenmodes of the optical branch (blue) and of the acoustical branch (red). (b) After summation on all eigenmodes, for the particles at the maxima of the potential (orange) and at the minima (green). The purple solid line is the averaged MSD for the whole chain. (c) Comparison between the MSD for a particle in a free chain (black solid line) and the averaged MSD for a chain in an asymmetric potential. The stiffnesses are $k = 1.27 \times 10^{-4}$ N m^{-1}, $k_1 = 1.67 \times 10^{-4}$ N m^{-1}, and $k_2 = 5.0 \times 10^{-4}$ N m^{-1}. There are $2N = 16$ particles, $\gamma = 10$ s^{-1}, and $T = 10^{10}$ K (see Sec. V B for an explanation of the temperature range).

modes still increases for a long time (red solid lines). Moreover, since most acoustical eigenfrequencies are smaller than those of a free chain, the corresponding saturation levels are higher than for the free chain.

Then, using Eq. (A10), the MSD $\langle \Delta x_\alpha^2(t) \rangle$ of a particle located respectively at a maximum ($\alpha = 1$) and a minimum ($\alpha = 2$) of the underlying potential can be calculated. The results are plotted in Fig. 3(b). As expected, the MSD of a particle located on a local maximum of the potential (solid red line) is much higher than that of a particle confined in a well of the underlying potential (solid green line), by typically three orders of magnitude.

The most striking effect is seen when one calculates the mean MSD of a particle in the chain (purple solid line). This is emphasized in Fig. 3(c), which displays a zoom on the relevant intermediate time range. This result evidences that the band gap opened by the underlying potential in the phonon spectrum (see Fig. 2) indeed enhances the fluctuations of the particles with respect to the case of a chain without an underlying potential.

We can then estimate the diffusivity D for underdamped systems and the mobility F for overdamped systems as in the case of the free chain. Our previous calculations, recalled in Eqs. (3) and (4), rely on the Debye approximation. This latter is still a good approximation when the chain interacts with an underlying potential for which k_1 and k_2 induce a frequency $\omega(q = 0)$ that is not too large, as shown by the inset in Fig. 2. Therefore, taking advantage of the expression of the acoustic eigenfrequency (11), the relevant expressions of the diffusivity and of the mobility are obtained simply by substituting k by $2k^2/\sqrt{(k_1+k_2)^2+16k^2}$ in Eqs. (3) and (4), which gives

$$D = \frac{k_B T}{\pi}\left[\frac{\sqrt{(k_1+k_2)^2+16k^2}}{2mk^2}\right]^{1/2}, \tag{14}$$

$$F = \frac{2k_B T}{\pi}\left[\frac{\sqrt{(k_1+k_2)^2+16k^2}}{m\gamma k^2}\right]^{1/2} = 2\sqrt{\frac{2}{\gamma}}D. \tag{15}$$

Note that the diffusivity and the mobility both increase with the width $(k_1 + k_2)$ of the band gap. This emphasizes once again the importance of this gap on the diffusion enhancement.

The asymmetry of the extremal curvatures of the potential is also of crucial importance. By comparing the coefficients obtained with [Eqs. (14) and (15)] and without [Eqs. (3) and (4)] the underlying potential, we obtain the dimensionless transport coefficients for $k = k_c$,

$$\frac{D}{D_0} = \frac{F}{F_0} = \left(\frac{k_1^2+k_2^2}{2k_1k_2}\right)^{1/2}. \tag{16}$$

In Fig. 4 these dimensionless transport coefficients are displayed as a function of the ratio k_1/k_2 which characterizes the potential asymmetry. The comparison of the simulations results with the simple estimate of Eq. (16) evidences a very good agreement. The enhancement of transport coefficients increases with the asymmetry of the potential extremal curvatures. Moreover, we can notice that in the case of a symmetric potential ($k_1/k_2 = 1$), the transport coefficients are the same with and without the potential. This explains why the enhancement of Brownian motion was not observed with a chain in a simple symmetric sinusoidal potential.

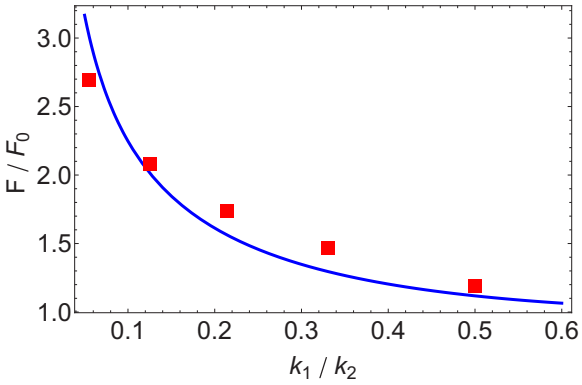

FIG. 4. Plot of the dimensionless mobility F/F_0 as a function of k_1/k_2. The red squares indicate the simulation results and the solid line is the theoretical estimates (16).

B. Effect of the underlying potential fluctuations: Effective temperature

Up to now we have considered a static underlying potential. However, in actual physical systems this potential may fluctuate, and the effect of these time fluctuations on the Browian motion of the particles has to be discussed.

Let us first consider a single diffusing particle of mass m in a harmonic potential of stiffness k. We introduce random fluctuations of this potential by assuming that the position of its minimum $\xi(t)$ is a random variable. The underlying potential to which the particle is submitted is thus

$$U(x,t) = \frac{k}{2}[x - \xi(t)]^2, \tag{17}$$

where the random variable has a vanishing mean value $\langle \xi(t) \rangle = 0$ and the statistical properties of a Gaussian white noise $\langle \xi(t)\xi(t') \rangle = \sigma^2 \delta(t - t')$ where σ is a real positive constant. The particle is submitted to a thermal bath of temperature T, described by a Gaussian fluctuating force $\mu(t)$ and a dissipation constant γ. The Langevin equation describing the motion of the particle is thus

$$\begin{aligned} m\ddot{x} &= -m\gamma\dot{x} - k[x - \xi(t)] + \mu(t) \\ &= -m\gamma\dot{x} - kx + \underbrace{k\xi(t) + \mu(t)}_{\mu_{\text{eff}}(t)}. \end{aligned} \tag{18}$$

In this equation, the fluctuating contribution can be considered as an effective noise $\mu_{\text{eff}}(t)$ which satisfies $\langle \mu_{\text{eff}}(t)\mu_{\text{eff}}(t') \rangle = 2k_B T_{\text{eff}} m\gamma\delta(t - t')$, defining an effective temperature

$$\frac{T_{\text{eff}}}{T} = \left(1 + \frac{k^2\sigma^2}{2k_B T m\gamma^2}\right). \tag{19}$$

This effective temperature is higher than the thermodynamic temperature, the additional contribution resulting from the transfer of fluctuations from the underlying potential to the particle system.

In order to test this analysis, we compare the probability distribution of particle positions $P(x)$ obtained in numerical simulations with the theoretical expectations for three values of σ (see Fig. 5). Each distribution is Gaussian, with the potential energy $U(x) = kx^2/2$ and an effective temperature taken as a fitting parameter. This effective temperature is plotted as

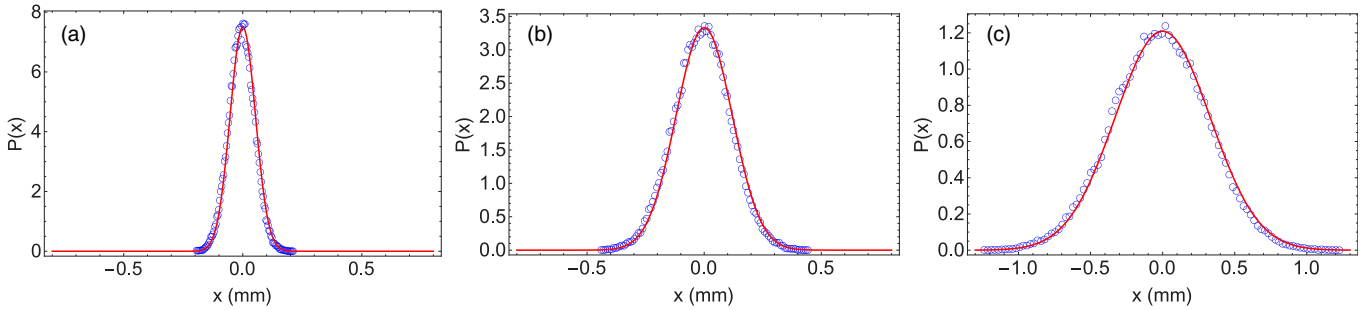

FIG. 5. Normalized probability distribution of the particle positions (mm) in a harmonic potential of stiffness $k = 5 \times 10^{-4}$ N m^{-1} for several amplitudes of the potential fluctuations: (a) $\sigma = 0.009$ mm, (b) $\sigma = 0.1$ mm, and (c) $\sigma = 0.3$ mm. The open blue dots are simulation data, and the dashed red lines are the equilibrium distributions in a static potential, using an effective temperature as a fitting parameter. The damping is $\gamma = 10$ s^{-1} and the thermodynamic temperature is $T = 10^{11}$ K.

a function of σ for two dissipation coefficients in Fig. 6. Regardless of the damping, the effective temperature is in excellent agreement with the function $T_{\rm eff}(\sigma)$ given by Eq. (19). This confirms that the diffusion of a particle in a fluctuating potential can be described by the diffusion of the same particle, in a static potential, but with a higher effective temperature.

Let us now consider the case of an underlying potential with asymmetrical extremal curvatures, assuming that each extremum location fluctuates independently of the others. The instantaneous displacements of the extrema $\alpha \in \{1,2\}$ of the jth cell will be denoted $\xi_j^\alpha(t)$, assuming that they are all independent Gaussian variables characterized by the same fluctuation amplitude σ. These fluctuations induce additional noise $\mu_j^\alpha|_{\rm eff}(t) = \mu_j^\alpha + k_\alpha \xi_j^\alpha(t)$ in the Langevin equations describing the dynamics of the particle positions $x_j^\alpha(t)$. After Fourier transforming the equations, linear combinations of such additional noise appear in the Langevin equations associated with the vibrational modes $X(q,t)$ of the chain of particles. Moreover, since this noise is all uncorrelated, it is easy to calculate the corresponding effective temperature which is the same regardless of the mode. This effective temperature $T_{\rm eff}$ is given by

$$\frac{T_{\rm eff}}{T} = 1 + \frac{(k_1^2 + k_2^2)\sigma^2}{4k_B T m \gamma^2}. \tag{20}$$

This effective temperature is higher than the actual (thermodynamic) one. There is a kind of fluctuation transfer from the underlying potential to the particles in the chain. Therefore, their diffusion is enhanced with respect to the case of a free chain.

Obviously, this effect strengthens the previous one associated with the gap opening. Taking into account these two effects, we inject in (14) and (15) the effective temperature (19) to get the ratios between the transport coefficients with the fluctuating underlying potential and the transport coefficients for the free chain at temperature T,

$$\frac{D(T_{\rm eff})}{D_0(T)} = \frac{F(T_{\rm eff})}{F_0(T)} = \left(\frac{k_1^2 + k_2^2}{2k_1 k_2}\right)^{1/2} \left(1 + \frac{k^2\sigma^2}{2k_B T m \gamma^2}\right). \tag{21}$$

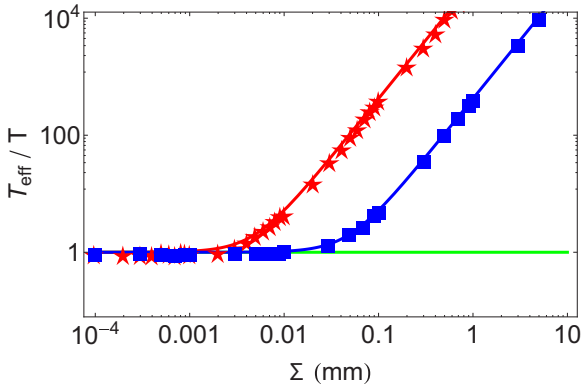

FIG. 6. Dimensionless effective temperature $T_{\rm eff}/T$ for a particle in a harmonic potential of stiffness $k = 5 \times 10^{-4}$ N m^{-1} as a function of the fluctuation amplitude of the potential well σ (mm), in logarithmic scale. The solid lines correspond to Eq. (19) while the discrete symbols are given by the fits of simulation data such as those displayed in Fig. 5. For $\gamma = 1$ s^{-1} (red crosses) and $\gamma = 10$ s^{-1} (blue squares).

V. COMPARISON WITH SIMULATION AND EXPERIMENTS

A. Effect of the band gap

In order to test our analysis of the effect of the band gap in the phonon spectrum on the particle MSD, we have undertaken numerical simulations. The details of the methods are given in our previous work [6], so here we restrict ourselves to a very brief summary.

We consider point particles of mass m located in the (x,y) plane at positions $\mathbf{r}_n = (x_n, y_n)$, submitted to a thermal bath at temperature T. Two particles at a distance r interact with a potential $U_{\rm int}(r) = U_0 K_0(r/\lambda_0)$, where U_0 is the energy scale, λ_0 is the potential range, and K_0 is the modified Bessel function of index 0. This peculiar choice of interaction potential corresponds to the interparticle interaction in the experiments which evidenced diffusion enhancement [24,42] (see Sec. V B). The particles are confined in the transverse direction y by a quadratic potential of stiffness β, in such a way that they cannot cross each other.

Let us first consider a static periodic potential with different curvatures for each extremum,

$$U(x) = \begin{cases} \frac{1}{2}k_2 x^2 & \text{if } |x| < \phi \text{ (modulo } 2d), \\ \frac{1}{2}k_2\phi d - \frac{1}{2}k_2\frac{\phi}{(d-\phi)}(d-x)^2 & \text{if } \phi < |x| < d \text{ (modulo } 2d), \end{cases} \tag{22}$$

where $2d$ and ϕ are respectively the potential period and the characteristic distance on which the curvature changes. It is easily checked that this potential is continuous with a continuous derivative at $x = \phi$. This is an example of a potential with asymmetric extremal curvatures, such as the one considered in Secs. III and IV, with

$$k_1 \equiv k_2 \frac{\phi}{(d-\phi)}, \tag{23}$$

so that by varying ϕ from 0 to d, we can tune the ratio k_1/k_2. For instance, for $\phi = d/2$, k_1 is equal to k_2. In order to have $k_1 < k_2$ and a stable configuration, we must have $\phi < d/2$. This potential is shown in Fig. 1 for a stiffness $k_2 = 8k_1$.

Each particle of index $n \in [1,2N]$ is submitted to a transverse confinement force $\beta y_n \mathbf{e}_y$, to the underlying forces $-U'(x_n)\mathbf{e}_x$, and to the interaction forces $-\boldsymbol{\nabla} U_{\text{int}}(|\mathbf{r}_m - \mathbf{r}_n|)$ from all other particles $m \neq n$. The dynamics of the nth particle is then given by the Langevin equations

$$m\ddot{\mathbf{r}}_n + m\gamma\dot{\mathbf{r}}_n + \sum_{m\neq n} \boldsymbol{\nabla} U_{\text{int}}(|\mathbf{r}_m - \mathbf{r}_n|) + U'(x_n)\mathbf{e}_x - \beta y_n \mathbf{e}_y = \mu(n,t), \tag{24}$$

with γ the damping constant and $\mu(n,t)$ the random force applied on the nth particle, which act independently on each particle, in each direction, and have the statistical properties of a white Gaussian noise.

Our simulations have been performed on a system of $2N = 16$ particles with periodic boundary conditions. We show in Fig. 7 the comparison between the average MSD of a particle as a function of time when the chain is embedded in an asymmetric potential, and when the chain is free. The comparison is done for three asymmetry ratios (k_1/k_2), with a stiffness $k \approx k_c$. The time evolution of the MSD is ballistic at small times for both the free chain and for the chain in an underlying potential. Eventually, the MSD scales as t for the free chain, whereas it saturates for the chain in an underlying potential (out of the time range of the figure). Between these two obvious asymptotic regimes, the MSD evidences correlations between the particles. The remarkable fact is that during this intermediate time regime, which extends on at least a decade, the average MSD is higher for the chain submitted to an asymmetric underlying potential than for the free chain.

For each asymmetry ratio, the MSD obtained in the simulations is in perfect agreement with the MSD calculated from the decomposition in phonons [see Eq. (A10)]. This confirms the validity of our model. We have identified the asymmetry of the extremal curvatures of the underlying potential as a relevant mechanism responsible for the enhancement of Brownian motion. Moreover, the greater the asymmetry ratio k_1/k_2, the greater is the enhancement of the MSD for the chain in an underlying potential compared to the free chain (notice that the ordinate scale is the same in all plots of Fig. 4), in agreement with Eq. (16).

B. The effective temperature

In order to test the effect of the underlying potential fluctuations on the particle diffusion, it is now convenient to return to experimental systems. Many of them are systems of coupled identical particles submitted to a thermal bath [16,17,24] in which two subsystems may be identified. It is thus possible to model one of the subsystems as an underlying potential applied to the other subsystem. The validity of such a modeling is not obvious and is carefully discussed in Appendix B.

As an example, we put the focus on *Wigner islands*, which are small lattices of a few tens of interacting particles confined in a disk and self-organized in concentric shells in which they diffuse without any crossing for a large range of temperature [24,44–47]. In the following, such a state will be denoted $N(N_1,N_2,N_3,\ldots)$, where N_j is the occupation number in the jth shell from the center. Such systems are particularly relevant because they are stable configurations that have been directly observed in a wide variety of systems, such as vortices in liquid helium [15], in Bose condensates [16], and in superconductors [17].

In particular, a very interesting and surprising phenomenon has been observed for $N = 19(1,6,12)$ Wigner islands in the intermediate time range. The orthoradial SFD of outer beads ($N_3 = 12$) is one order of magnitude higher than in a system of 12 beads diffusing in a smooth annulus of *the same* radius [42]. Let us emphasize that in these experimental results, the long time behavior has not been reached. Indeed, the relevant crossover time is proportional to the dissipation coefficient [6] which is large in these experiments. Furthermore, by exploring the effect of commensurability N_3/N_2 on the amplitude of this effect with $N = 18(1,6,11)$ and $N = 20(1,6,13)$ systems, the authors had suggested that a possible explanation for this puzzling effect is that the beads in the outer shell are submitted to the modulated and fluctuating quasi-one-dimensional (1D) potential created by the inner beads.

In order to understand the origin of the periodic potential imposed by the inner beads onto the beads in the outer shell, it is convenient to recall the relevant setup of these experiments (for details, see Ref. [47]). It consists of electrostatically interacting conducting beads of millimeter size located on the bottom electrode of a horizontal plane capacitor, while the top electrode is a transparent conductor allowing the video recording of the motion of the beads. The beads are transversally confined by another potential applied to a metallic isolated circular frame. The temperature is simulated by mechanical shaking. When an electrical tension of about 1000 V is applied, the metallic beads become charged and interact between themselves [24,42,47]. This interparticle interaction $U_0 K_0(r/\lambda_0)$ has been analytically calculated and gives an excellent agreement between the observed and the calculated Wigner islands [48].

This interaction allows for the calculation of the potential energy induced by the six inner beads and the circular

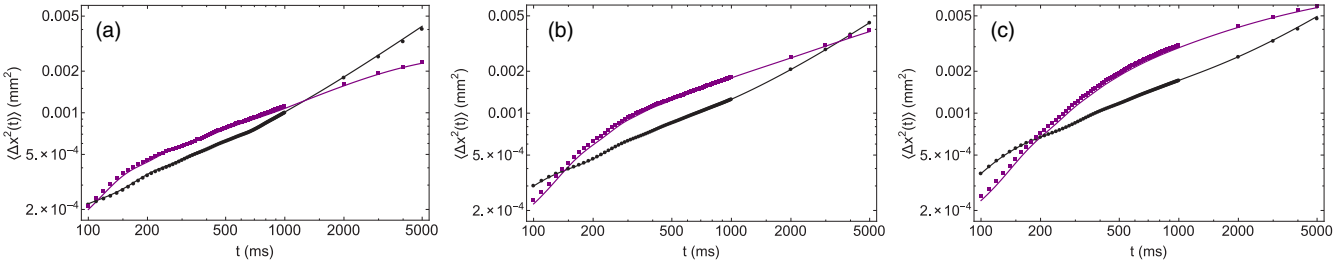

FIG. 7. Plot of the average MSD (mm^2, logarithmic scale) as a function of time (ms, logarithmic scale). The dots are simulation data (purple squares: chain in an underlying potential; black disks: free chain), and the solid lines are the theoretical calculations using the phonon decomposition. In all cases there are $2N = 16$ particles, $\gamma = 10\ s^{-1}$, and $T = 10^{10}$ K. In units of 10^{-3} N m^{-1}, the relevant stiffnesses are (a) $k = 1.26$, $k_1 = 1.67$, and $k_2 = 5$ ($k_1/k_2 = 0.33$), (b) $k = 0.685$, $k_1 = 1.1$, and $k_2 = 5$ ($k_1/k_2 = 0.21$), and (c) $k = 0.36$, $k_1 = 0.625$, and $k_2 = 5$ ($k_1/k_2 = 0.125$).

confinement on the 12 beads of the outer shell. Several equipotentials are displayed in Fig. 8. These curves exhibit a periodic modulation with the polar angle θ, particularly the equipotential $V^*(\theta)$ that corresponds to the minimum of the potential (green solid line).

The amplitude and the local curvatures of $V^*(\theta)$ felt by the outer beads are both plotted as a function of the polar angle θ in Fig. 9 [49]. This potential exhibits different stiffnesses at its maxima and minima, with the absolute value of stiffness at the maxima being smaller than at the minima. The ratio k_1/k_2 is roughly 0.3, and the stiffness between particles in the outer shell is $k \sim 5.4 \times 10^{-5}$ N m^{-1} while $k_c \sim 4.5 \times 10^{-5}$ N m^{-1}. Note that the stable Wigner island pattern, with beads in the outer shell that alternate between the maxima and the minima of the potential due to the inner shell, is consistent with the stability analysis of Sec. III which requires $k_1 < k_2$ and $k > k_c$.

If this potential were static, according to the theoretical calculation of Sec. IV A, a ratio $k_1/k_2 \sim 0.3$ should induce a ratio of mobilities $F(T)/F_0(T)$ around 1.3 (see Fig. 4). However, the experiments performed on this system give a mobility ratio of around 10 (see Ref. [42], Fig. 3). The asymmetry of the extremal curvatures of the experimental potential actually results in an increase of the particle mobility, in qualitative agreement with the effect discussed in Sec. V A. However, the magnitude of the diffusion enhancement is not fully recovered with only this contribution, and the fluctuation transfer has to be taken into account.

As discussed in Sec. IV B, an effective temperature for the outer shell can be defined. Quantitatively, in the experiments, the inner beads are located on a ring of radius 2.2 mm and have a mass $m = 2.1$ mg. The mean square orthoradial motion of the inner beads is roughly 10^{-3} rad^2 (see Ref. [42], Fig. 2). Therefore, an estimate of the MSD σ^2 for the random variable $\xi(t)$ defined in Eq. (17) is roughly 4×10^{-9} m^2. The experiments have been performed at 10^{12} K [50] and the dissipation coefficient was $\gamma = 10$. With these data, the ratio $F(T_{\rm eff})/F_0(T)$ calculated using Eq. (21) is roughly 30. This order of magnitude is very satisfactory, if we take into account the crudeness of the estimate provided in Eq. (21), which relies on qualitative arguments that were only validated for fluctuating quadratic potentials.

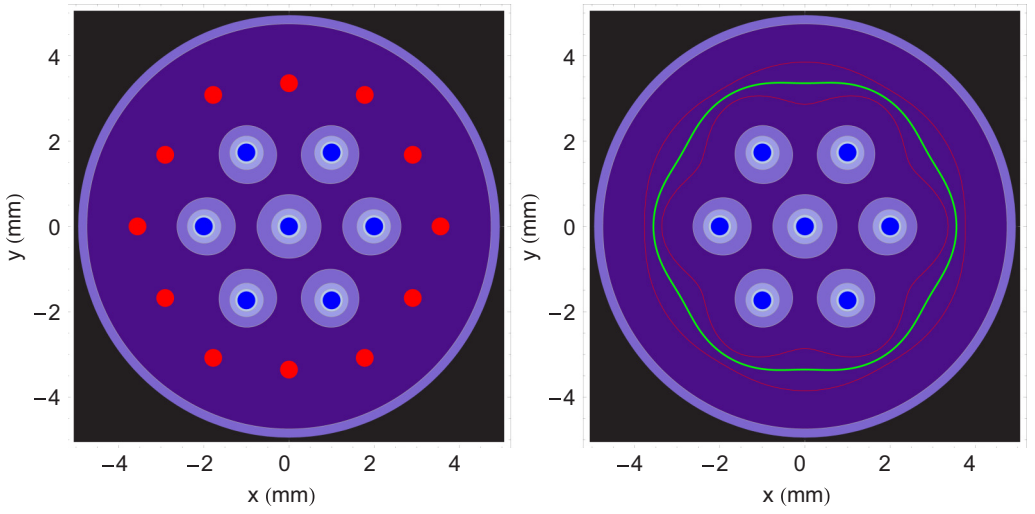

FIG. 8. Left: Wigner island $N = 19(1,6,12)$. Blue dots: inner particles; red dots: outer particles. The purple color scale corresponds to the potential energy amplitude. Right: The purple color scale corresponds to the potential energy resulting from the inner particles and the circular confinement. The red solid lines are two equipotentials, and the green solid line indicates the location of the potential minimum.

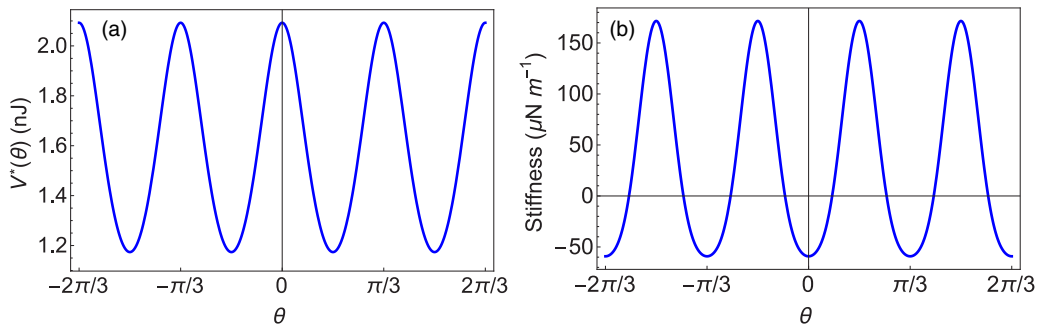

FIG. 9. (a) Potential energy $V^*(\theta)$ (nJ) along the minimum equipotential, as a function of the polar angle θ. (b) Local stiffness (μN m^{-1}) as a function of the polar angle θ.

VI. CONCLUSION

While the single file diffusion (SFD) of a chain of interacting particles in a smooth confining channel is well known, the effects of corrugations and fluctuations of the confining potential on the particle dynamics is less studied. Nevertheless, it was recently exhibited that, in the time range during which the Brownian motions of these particles are correlated, their mean squared displacement (MSD) can be larger in a corrugated channel than in a smooth one. It was suggested that this surprising enhancement could be attributed to these corrugations and their fluctuations.

In this article, we put the focus on the modification of the SFD induced by an underlying periodic potential that models the channel corrugations, taking into account its time fluctuations as well. For the sake of comparison with experiments, we have restricted our study to systems in which the underlying potential and the chain have commensurate periods and to low temperatures for which the particles' MSD remains smaller than the potential period. In such conditions, the system of interacting particles may be described by a set of identical masses linked by springs of identical stiffnesses.

The transport coefficients for SFD are calculated by a projection on the phonon basis of the particles' chain. Each phonon behaves as a (fictitious) particle in a harmonic potential, with a stiffness that is given by its phonon frequency. Its MSD increases at a small time and saturates at a long time to a value inversely proportional to its stiffness. The MSD of a particle in the chain is just a weighted sum of the phonon MSD. In this framework, the SFD behavior of the MSD results from the progressive saturation of each phonon MSD. When the periodic potential is applied on the chain, the changes in the vibrational spectrum modify the transport coefficients.

When the periods of the chain and of the underlying potential are identical, all the particles are trapped in the potential minima. This implies an increase in the stiffnesses, hence an increase in the phonon frequencies. Therefore, the phonons' MSD saturation is faster and the transport coefficients of the particles decrease.

A more interesting configuration is a commensurate system with two particles per potential period. In this case, the particles' Brownian motion is enhanced. We have exhibited that the key point to understanding this effect is to consider that the curvature at a potential minimum is larger than the absolute value of the curvature at a potential maximum. In this case, one half of the particles are located near the minima and one half near the maxima. This configuration is consistent with actual systems (the so-called Wigner islands) in which "diffusion enhancement" has been observed. In such systems, a gap is opened at the band edges of the phonon spectrum so that the frequencies of the acoustical modes are smaller than for the free chain. Therefore, they saturate at longer times and the SFD evidenced at intermediate times is enhanced.

When the underlying potential undergoes time fluctuations, a fluctuation transfer occurs with the chain, which behaves as if it were in a thermal bath with a larger temperature. This larger effective temperature strengthens the opening gap effect and implies even larger transport coefficients for the particles in the underlying potential. When the time fluctuations of the underlying potential are taken into account by the corresponding effective temperature, we recover the order of magnitude of the diffusion enhancement observed in previous experiments.

These results exhibit the peculiar role played by the particles near the potential maxima in this enhancement of Brownian motion. Up to now, this kind of approach can be extended to other commensurate configurations in which diffusion enhancement has been observed. However, very similar effects can be also expected in incommensurate systems since, in such systems, incommensurability inevitably results in the presence of some particles near these maxima.

APPENDIX A: PHONON DECOMPOSITION AND SFD

In this Appendix, we generalize the particles' MSD calculations of Ref. [6] to the case of particles in a chain in an external periodic potential. When the chain is in a thermal bath and interacts with an external potential such as in Fig. 1, Eqs. (5) are replaced by

$$\begin{cases} m\ddot{x}_j^1 = -m\gamma\dot{x}_j^1 + k\left(x_j^2 + x_{j-1}^2 - 2x_j^1\right) + k_1 x_j^1 + \mu_j^1, \\ m\ddot{x}_j^2 = -m\gamma\dot{x}_j^2 + k\left(x_{j+1}^1 + x_j^1 - 2x_j^2\right) - k_2 x_j^2 + \mu_j^2, \end{cases} \tag{A1}$$

with a thermal noise such that

$$\left\langle \mu_j^\alpha(t) \right\rangle = 0, \quad \left\langle \mu_j^\alpha(t)\mu_{j'}^\beta(t') \right\rangle = g\delta_{jj'}\delta_{\alpha\beta}\delta(t-t'), \tag{A2}$$

where $\langle\cdot\rangle$ means statistical averaging and where $g \equiv 2m\gamma k_B T$. After the Fourier transform, the dynamics of the phonons is given by

$$\ddot{\mathbf{X}} = -\gamma\dot{\mathbf{X}} + \mathbb{M}(s)\mathbf{X}(s,t) + \widehat{\mathbf{M}}(s,t), \tag{A3}$$

where the Hermitian matrix $\mathbb{M}$ is defined in Eq. (8), where $\mathbf{X} \equiv (X_1, X_2)^T$, and where $(\cdots)^T$ indicates matrix transposition.

The two components of the noise vector $\widehat{\mathbf{M}}(s,t) \equiv (\widehat{\mu}^1,\widehat{\mu}^2)^T$ are the Fourier transforms of $\mu^\alpha(t)$,

$$\widehat{\mu}^\alpha(s,t) = \sum_{j=1}^{N} \mu_j^\alpha(t) e^{-i\frac{2\pi}{N}sj}, \tag{A4}$$

which are easily seen to verify

$$\langle \widehat{\mu}^\alpha \rangle = 0, \quad \langle \widehat{\mu}^\alpha(s,t)\widehat{\mu}^\beta(-s,t')\rangle = Ng\delta_{\alpha\beta}\delta(t-t'). \tag{A5}$$

Introducing the unitary matrix $\mathbb{P} \equiv (\mathbf{V}_+,\mathbf{V}_-)$ where the eigenvectors $\mathbf{V}_\pm$ are defined in Eq. (10), we readily obtain from Eq. (A3),

$$\mathbb{P}^{-1}\ddot{\mathbf{X}} = -\gamma\mathbb{P}^{-1}\dot{\mathbf{X}} + \mathbb{D}(s)\mathbb{P}^{-1}\mathbf{X}(s,t) + \mathbb{P}^{-1}\widehat{\mathbf{M}}(s,t), \tag{A6}$$

where $\mathbb{D}(s)$ is the diagonal matrix,

$$\mathbb{D}(s) = \begin{pmatrix} -m\omega_+^2(s) & 0 \\ 0 & -m\omega_-^2(s) \end{pmatrix}. \tag{A7}$$

Each phonon is a component of the vector $\mathbb{P}^{-1}\mathbf{X}(s,t)$, and it is seen from Eq. (A6) that its dynamics is that of a particle in a harmonic potential of stiffness $m{\omega_\pm}^2(s)$, submitted to a thermal bath which is the relevant component of $\widetilde{\mathbf{M}}$. It remains to establish that the phonons undergo uncorrelated thermal noises.

Let $\widetilde{\mathbf{M}}(s,t) \equiv (\widetilde{\mu}^1,\widetilde{\mu}^2)^T = \mathbb{P}^{-1}\widehat{\mathbf{M}}(s,t)$. The statistical average of each component of $\widetilde{\mathbf{M}}$ obviously vanishes. The correlations of the noise terms in Eq. (A6) are then found to be

$$\begin{aligned}\langle \widetilde{\mu}^\alpha(s,t)\widetilde{\mu}^\beta(-s,t')\rangle &= \left\langle \mathbb{P}^{-1}_{\alpha\gamma}(s)\widehat{\mu}^\gamma(s,t)\mathbb{P}^{-1}_{\beta\eta}(-s)\widehat{\mu}^\eta(-s,t')\right\rangle \\ &= \mathbb{P}^{-1}_{\alpha\gamma}(s)\mathbb{P}^{-1}_{\beta\gamma}(-s)Ng\delta(t-t'),\end{aligned} \tag{A8}$$

where we assume a summation on repeated greek indices and where we have used Eq. (A5). Now $\mathbb{P}^{-1}_{\beta\gamma}(-s) = \mathbb{P}^{-1*}_{\beta\gamma}(s)$, where $(\cdots)^*$ means complex conjugation. Taking into account the unitarity of the matrix $\mathbb{P}$, we get

$$\begin{aligned}\langle \widetilde{\mu}^\alpha(s,t)\widetilde{\mu}^\beta(-s,t')\rangle &= \mathbb{P}^{-1}_{\alpha\gamma}(s)\mathbb{P}_{\gamma\beta}(s)Ng\delta(t-t') \\ &= Ng\delta_{\alpha\beta}\delta(t-t'),\end{aligned} \tag{A9}$$

which proves that the thermal noise applied to the phonons is indeed uncorrelated.

It is thus a simple task to calculate the MSD of each phonon, as in Ref. [6]. The MSD of a particle is then easily calculated by taking into account the relative weight of each phonon in its motions, and reads

$$\left\langle \Delta x_\alpha^2(t)\right\rangle = \frac{1}{N^2}\sum_{s=1}^{N}\sum_{\beta=1}^{2}|\mathbb{P}_{\alpha\beta}(s)|^2\left\langle \Delta X_\beta^2(s,t)\right\rangle. \tag{A10}$$

Because of translational invariance, it does not depend on the cell index, but it obviously depends on the particle equilibrium position being at a maximum of the underlying potential ($\alpha = 1$) or at a minimum ($\alpha = 2$).

APPENDIX B: THE UNDERLYING POTENTIAL MODEL

In Sec. V B, we model the motion of the outer shell in a Wigner island as that of a chain of particles in a modulated underlying potential, induced by the beads in the inner shells. This description is far from obvious, because the Wigner island is a coupled system, and the motions of the beads in the inner shell depend upon the beads in the outer shell, and it is not strictly correct to interpret the potential created by the inner beads as *external*.

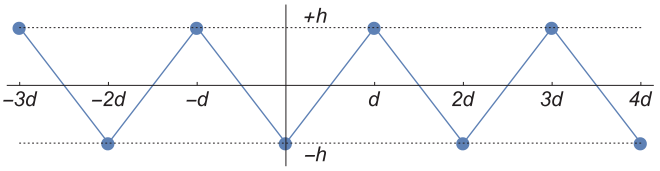

FIG. 10. Sketch of a zigzag pattern. The solid line is a guide for the eye.

In order to show that the dynamics of two coupled chains can be described despite these differences as the diffusion of one chain in an underlying potential, we consider a *zigzag pattern* [51,52]. Such patterns are observed in quasi-one-dimensional systems of transversally confined repelling particles. When the transverse confinement is reduced, it eventually becomes energetically favorable for the particles to distribute in a staggered row, as shown in Fig. 10. This system can either be considered as a staggered row of $2N$ particles with longitudinal distance d and transverse width $2h$, or as a system of two chains of N particles, with a longitudinal distance $2d$, separated by a transverse distance $2h$. The aim of this Appendix is to show that it is possible to describe it quite correctly, although in an approximate way, as one chain of N particles in a periodic underlying potential that models the other chain.

We compare the longitudinal MSD for particles calculated from the modes of vibration of the zigzag configuration as a whole [53] to the longitudinal MSD obtained by simulation of the diffusion of a chain in an underlying periodic potential. The effect of the thermal fluctuations on the underlying potential are accounted for by a single random variable that defines the location of one local maximum of the potential, which is assumed to have the constant period $2d$.

The underlying potential is assumed to be sinusoidal of period $2d$ with an amplitude ΔE that depends on the width h of the zigzag pattern and that characterizes the coupling between the two chains. The particles of the diffusing chain are located near the potential minima separated by a mean distance $2d$, with a local stiffness $\pi^2\Delta E/d^2$. Since we restrict ourselves to temperatures low enough for the zigzag pattern to be stable, the relative displacement of a particle of one chain with respect to its neighbors in the other chain is always smaller than the interparticle distance d. Therefore, we have only considered small random longitudinal displacements of the underlying potential. This random displacement has been simulated by that of a single free particle of mass $2Nm$ (in other terms, we just consider the fluctuations of large wavelength) diffusing at a low temperature in one well of the periodic potential. The amplitude ΔE is taken as a fitting parameter, which is then compared to the calculated barrier height $\Delta E(h)$ for the actual zigzag pattern.

The comparison between the actual diffusion of the particles in a zigzag pattern and the model of a chain in an underlying potential is done in Fig. 11, for a pattern with $2N = 16$ particles. We consider two damping constants γ, and two values of the transverse height h. As expected, the MSD

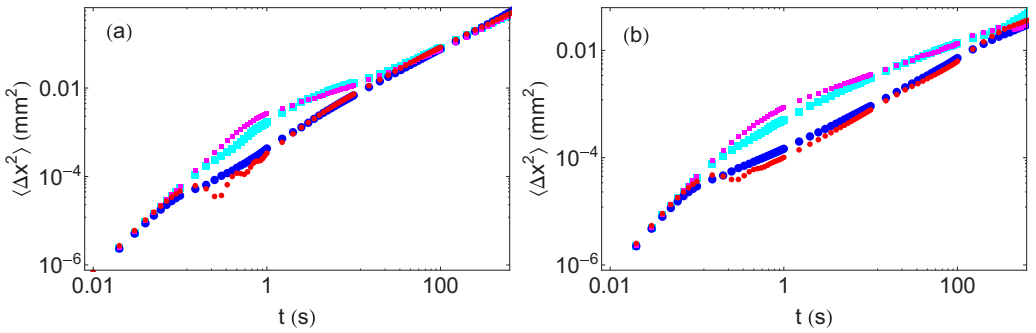

FIG. 11. Longitudinal MSD for a particle in a zigzag pattern ($2N = 16$; blue dots for $h = 0.10$ mm, cyan squares for $h = 0.78$ mm) and for a particle in a chain with an underlying potential ($N = 8$; red dots, magenta squares) for a temperature $T = 10^9$ K. The dissipation constants are (a) $\gamma = 1$ s^{-1} and (b) $\gamma = 10$ s^{-1}. The fitting parameter is $\Delta E = 6.0 \times 10^2$ nJ for the red dots, to be compared to a barrier height of $\Delta E = 1.6 \times 10^2$ nJ for the corresponding zigzag pattern (blue dots). The fitting parameter is $\Delta E = 0.6$ nJ for the magenta squares, to be compared to a barrier height of $\Delta E = 1.7$ nJ for the corresponding zigzag pattern (cyan squares).

resembles that of a single free chain for large h whereas it is much smaller for small h.

Most importantly, for both values of h and γ, the actual MSD for the zigzag system and the MSD for the model system are in good agreement since the actual barrier height compares very well with the fitting parameter ΔE. This agreement between the MSD calculated for the actual zigzag pattern and the MSD calculated for a single chain in an underlying periodic and fluctuating potential validates the description used in Sec. IV.

[1] D.W. Jepsen, Dynamics of a simple many-body system of hard rods, J. Math. Phys. **6**, 405 (1965).

[2] R. Arratia, The motion of a tagged particle in the simple symmetric exclusion system on Z, Ann. Probab. **11**, 362 (1983).

[3] K. Hahn and J. Kärger, Deviations from the normal time regime of single file diffusion, J. Phys. Chem. B **102**, 5766 (1998).

[4] M. Kollmann, Single-File Diffusion of Atomic and Colloidal Systems: Asymptotic Laws, Phys. Rev. Lett. **90**, 180602 (2003).

[5] B. U. Felderhof, Fluctuation theory of single-file diffusion, J. Chem. Phys. **131**, 064504 (2009).

[6] J.-B. Delfau, C. Coste, and M. S. Jean, Single file diffusion of particles with long-ranged interactions: Damping and finite size effects, Phys. Rev. E **84**, 011101 (2011).

[7] P. C. Bressloff and J. M. Newby, Stochastic models of intracellular transport, Rev. Mod. Phys. **85**, 135 (2013).

[8] A. Ryabov, *Stochastic Dynamics and Energetics of Biomolecular Systems* (Springer, Berlin, 2016).

[9] K. Falk, F. Sedlmeier, L. Joly, R. R. Netz, and L. Bocquet, Molecular origin of fast water transport in carbon nanotube membranes, Nano Lett. **10**, 4067 (2010).

[10] P. Demontis, G. Stara, and G. B. Suffritti, Dynamical behavior of one-dimensional water molecule chains in zeolites: Nanosecond time-scale molecular dynamics simulations of bikitaite, J. Chem. Phys. **120**, 9233 (2004).

[11] C. Lutz, M. Kollmann, P. Leiderer, and C. Bechinger, Diffusion of colloids in one-dimensional light channels, J. Phys.: Condens. Matter **16**, S4075 (2004).

[12] C. Lutz, M. Kollmann, and C. Bechinger, Single-File Diffusion of Colloids in One-Dimensional Channels, Phys. Rev. Lett. **93**, 026001 (2004).

[13] B. Lin, M. Meron, B. Cui, S. A. Rice, and H. Diamant, From Random Walk to Single-File Diffusion, Phys. Rev. Lett. **94**, 216001 (2005).

[14] P. Henseler, A. Erbe, M. Köppl, P. Leiderer, and P. Nielaba, Density reduction and diffusion in driven two-dimensional colloidal systems through microchannels, Phys. Rev. E **81**, 041402 (2010).

[15] E. J. Yarmchuk and R. E. Packard, Photographic studies of quantized vortex line, J. Low Temp. Phys. **46**, 479 (1982).

[16] K. W. Madison, F. Chevy, W. Wohlleben, and J. Dalibard, Vortex Formation in a Stirred Bose-Einstein Condensate, Phys. Rev. Lett. **84**, 806 (2000).

[17] N. Kokubo, S. Okayasu, A. Kanda, and B. Shinozaki, Scanning SQUID microscope study of vortex polygons and shells in weak-pinning disks of an amorphous superconducting film, Phys. Rev. B **82**, 014501 (2010).

[18] S. Anders, A. W. Smith, H. M. Jaeger, R. Besseling, P. H. Kes, and E. van der Drift, Commensurability effects and fluctuations of vortex flow in mesoscopic channels, Physica C **332**, 35 (2000).

[19] N. Kokubo, R. Besseling, V. M. Vinokur, and P. H. Kes, Mode Locking of Vortex Matter Driven through Mesoscopic Channels, Phys. Rev. Lett. **88**, 247004 (2002).

[20] N. Kokubo, R. Besseling, and P. H. Kes, Dynamic ordering and frustration of confined vortex rows studied by mode-locking experiments, Phys. Rev. B **69**, 064504 (2004).

[21] C. Fusco, A. Fasolino, and T. Janssen, Nonlinear dynamics of dimers on periodic substrates, Eur. Phys. J. B **31**, 95 (2003).

[22] C. Fusco and A. Fasolino, Microscopic mechanisms of thermal and driven diffusion of non rigid molecules on surfaces, Thin Solid Films **428**, 34 (2003).

[23] E. Heinsalu, M. Patriarca, and F. Marchesoni, Dimer diffusion in a washboard potential, Phys. Rev. E **77**, 021129 (2008).

[24] G. Coupier, M. S. Jean, and C. Guthmann, Single file diffusion in macroscopic Wigner rings, Phys. Rev. E **73**, 031112 (2006).

[25] C. A. Wert, Diffusion coefficient of C in α-iron, Phys. Rev. **79**, 601 (1950).
[26] P. Brüesh, L. Pietronero, S. Strässler, and H. R. Zeller, Brownian motion in a polarizable lattice: Application to superionic conductors, Phys. Rev. B **15**, 4631 (1977).
[27] S. Bleil, P. Reimann, and C. Bechinger, Directing Brownian motion by oscillating barriers, Phys. Rev. E **75**, 031117 (2007).
[28] W. Mu, Z. Liu, L. Luan, G. Wang, G. C. Spalding, and J. B. Ketterson, Enhanced particle transport in an oscillating sinusoidal optical potential, New J. Phys. **11**, 103017 (2009).
[29] L. Gunther, M. Revzen, and A. Ron, Mobility in a periodic potential: A simple derivation, Physica A **95**, 367 (1979).
[30] H. Risken, *The Fokker-Planck Equation* (Springer, Berlin, 1989).
[31] D. Reguera and J. M. Rubi, Kinetic equations for diffusion in the presence of entropic barriers, Phys. Rev. E **64**, 061106 (2001).
[32] P. Kalinay and J. K. Percus, Corrections to the Fick-Jacobs equation, Phys. Rev. E **74**, 041203 (2006).
[33] P. S. Burada, P. Hänggi, F. Marchesoni, G. Schmid, and P. Talkner, Diffusion in confined geometries, Chem. Phys. Chem. **10**, 45 (2009).
[34] A. Taloni and F. Marchesoni, Collisional statistics of a stochastic single file, Phys. Rev. E **74**, 051119 (2006).
[35] O. M. Braun and Y. S. Kivshar, Nonlinear dynamics of the Frenkel-Kontorova model, Phys. Rep. **306**, 1 (1998).
[36] S. Herrera-Velarde and R. Castaneda-Priego, Structure and dynamics of interacting Brownian particles in one-dimensional periodic substrate, J. Phys.: Condens. Matter **19**, 226215 (2007).
[37] S. Herrera-Velarde and R. Castañeda-Priego, Superparamagnetic colloids confined in narrow corrugated substrates, Phys. Rev. E **77**, 041407 (2008).
[38] X. Yang, M. Wu, Z. Qin, J. Wang, and T. Wen, Molecular dynamics simulations on single-file diffusions: Effects of channel potential periods and particle-particle interactions, J. Appl. Phys. **106**, 084905 (2009).
[39] D. Lucena, J. E. Galván-Moya, W. P. Ferreira, and F. M. Peeters, Single-file and normal diffusion of magnetic colloids in modulated channels, Phys. Rev. E **89**, 032306 (2014).
[40] J.-B. Delfau, C. Coste, and M. S. Jean, Enhanced fluctuations of interacting particles confined in a box, Phys. Rev. E **85**, 041137 (2012).
[41] C. Coste, J.-B. Delfau, C. Even, and M. S. Jean, Single file diffusion of macroscopic charged particles, Phys. Rev. E **81**, 051201 (2010).
[42] G. Coupier, M. S. Jean, and C. Guthmann, Single file diffusion enhancement in a fluctuating modulated quasi-1D channel, Europhys. Lett. **77**, 60001 (2007).
[43] Because of the translational invariance, the MSD does not depend on the cell index j, but it depends on the particle being at a maximum ($\alpha = 1$) or at a minimum ($\alpha = 2$) of the underlying potential.
[44] L. J. Campbell and R. M. Ziff, Vortex patterns and energies in a rotating superfluid, Phys. Rev. B **20**, 1886 (1979).
[45] V. M. Bedanov and F. M. Peeters, Ordering and phase transitions of charged particles in a classical finite two-dimensional system, Phys. Rev. B **49**, 2667 (1994).
[46] Y.-J. Lai and Lin I, Packings and defects of strongly coupled two-dimensional Coulomb clusters: Numerical simulation, Phys. Rev. E **60**, 4743 (1999).
[47] G. Coupier, C. Guthmann, Y. Noat, and M. S. Jean, Local symmetries and order-disorder transitions in small macroscopic Wigner islands, Phys. Rev. E **71**, 046105 (2005).
[48] P. Galatola, G. Coupier, M. S. Jean, J.-B. Fournier, and C. Guthmann, Determination of the interactions in confined macroscopic Wigner islands: Theory and experiments, Eur. Phys. J. B **50**, 549 (2006).
[49] When this potential $V(r,\theta)$ is calculated at the minimum of the potential energy, hence on the curve $r^*(\theta)$, its value $V[r^*(\theta),\theta] \equiv V^*(\theta)$ is indeed a function of the polar angle only.
[50] Let us remind the reader that this is an *effective* temperature, and that for macroscopic particles the corresponding thermal energy is roughly 10% of the average interaction energy.
[51] T. Dessup, T. Maimbourg, C. Coste, and M. S. Jean, Linear instability of a zigzag pattern, Phys. Rev. E **91**, 022908 (2015).
[52] T. Dessup, C. Coste, and M. S. Jean, Subcriticallity of the zigzag transition: A nonlinear bifurcation analysis, Phys. Rev. E **91**, 032917 (2015).
[53] T. Dessup, Instabilités et dynamiques de particules en interaction dans un système quasi-unidimensionnel, Ph.D. thesis, Université Paris Diderot, 2016, https://hal-univ-diderot.archives-ouvertes.fr/tel-01404418.